Change Detection Methods in High Resolution Cosmo SkyMed images

Sofia Lanfri[1], Marcelo Scavuzzo[1], Mario A. Lanfri[1], Gabriela Palacio[2], Alejandro C. Frery[3]
[1]Instituto Mario Gulich, Comisión Nacional de Actividades Espaciales, Córdoba, Argentina
Ruta C45 km 8, Falda del Cañete, slanfri@conae.gov.ar
[2]Universidad Nacional de Río Cuarto, Córdoba, Argentina
[3]Universidade Federal de Alagoas, Maceió, AL, Brazil

***Abstract*—In this paper we compare three approaches for change detection in SAR imagery: GRLT, MIMOSA and one based on the Hellinger stochastic distance between distributions. The comparison is made using COSMO-SkyMed images from which training samples from four types of areas subjected to change, and from two areas which underwent no change. Whereas GRLT and the Hellinger distance-based procedures yielded good results, MIMOSA failed at detecting the changes.**

I. Introduction

Research about multi-temporal image analysis has been expanded because of the increasing availability of data from Synthetic Aperture Radar (SAR) satellites with characteristics such as short revisit time, all-day and all-weather acquisitions. The COSMO-SkyMed (CSK) constellation consist of four satellites having less than 12 hours revisit time. It represents a remarkable data source to be used on change detection applications.

Change detection is based on the comparison of two or more images from the same scene acquired at different dates, seeking for change indicators or dissimilarity measures for each pair of pixels. Classical change detectors can be grouped in two categories: 1) considering only the pixel intensity of the images, and 2) considering local statistics in the pixel neighborhood. Change operators are also divided according to the number of temporal images employed [1].

Because of the multiplicative nature of speckle in SAR, which can induce false alarms, classical methods use local statistics in the neighborhood of each pixel. The standard detector is based on the Log-Ratio [2]–[5] that computes the ratio of the local means in an image pair. However, if the change preserves the mean value modifying only the local texture (modeled as a zero-mean multiplicative contribution [6]), it will not be detected. The ratio of means would be useful to recognize step changes whereas higher order statistics would be suitable to detect progressive changes in multi-temporal series [5].

Generalized Likelihood Ratio Test (GLRT) [1], [7], Log-cumulants for spatio-temporal heterogeneity [5], Local statistics Similarity Measures [4] and InformationTheoretic approaches [8], [9] are also applied as change indicators.

In this work, the performance of three different change detection approaches for CSK images is evaluated. The compared methodologies are: 1) Generalized Likelihood Ratio Test (GLRT) [1], [7], 2) MIMOSA approach proposed in [10], and 3) Information theory separability measures, e.g. stochastic distances and their derived hypothesis tests [11]. The assessment considers various change levels: abrupt changes (e.g. deforestation), evolutionary changes (e.g. vegetation areas), no-change, i.e., stable areas (e.g. urban regions), and periodic changes (e.g. vegetation phenology).

II. Methodology

The data set consists of two CSK-3 images, provided under the ASI–CONAE SIASGE agreement. The study area is Foz do Iguazú region, Paraná, Brazil (Fig. 1). The images used were acquired with identical geometrical characteristics: 29° incidence angle, right acquisition, descendant orbit, Stripmap Himage (HI) mode of about $3\,\mathrm{m}$ of nominal resolution. The images were acquired on 2011/04/11 and on 2011/10/20.

The CSK data was preprocessed to obtain intensity calibrated data: $\sigma^o = K^{-1}\sin\alpha_{REF} R_{REF}^{2j} F_R^{-2} P_i^2$, where R_{REF} is the slant-range reference distance, j is the reference slant range exponent, α_{REF} is the reference incidence angle, F_R is the rescaling factor, K is the calibration constant, and P_i is the CSK image amplitude value. Both CSK image were coregistered using the ENVI 4.7 software, using both automatic and manual control points.

A. Assessed methodologies

For the following three methods, coregistered SAR intensity images acquired at different dates were analyzed, and a map identifying the intensity of the change between images (**change map**) was developed. All the methods used a 7×7 sliding window, and the implementations were carried out in the R platform (http://www.r-project.org/) for enhanced numerical properties [12].

1) Generalized Likelihood Ratio Test (GLRT) [1]: This methodology is based on testing H_0 : there is no change against H_1 : the first image intensity comes from an underlying reflectivity $\hat\lambda_1$ which is different from the reflectivity of the second image $\hat\lambda_2$.

Homogeneous areas in intensity format can be described by using the multiplicative model [13]. Torres et al. [14] model the heterogeneity using a Gamma distribution allowing the number of looks to vary locally. The distribution of the

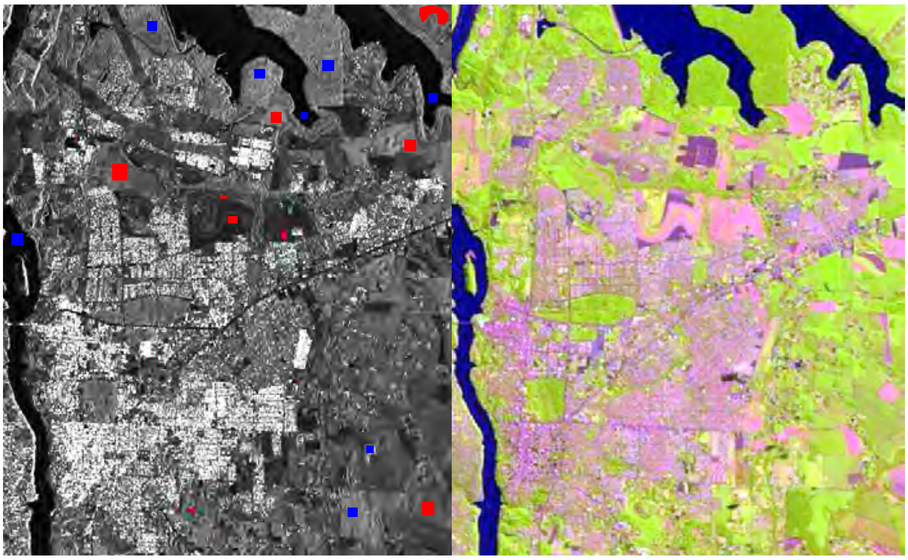

(a) CSK 3 image. Selected regions of *change* in red, and *no-change* in blue.

(b) Landsat 5 TM image dated April 24, 2011. Source: Landsat/USGS.

Fig. 1. Study area in Foz do Iguazú region, Paraná, Brazil.

observed multilook intensity data follows, then, a gamma random variable with density

$$f_Z(z;L,\lambda)=\frac{L^L}{\lambda^L\Gamma(L)}z^{L-1}\exp\left\{\frac{-Lz}{\lambda}\right\},$$

where Γ is the gamma function, $z,\lambda>0$ and $L>0$ is the equivalent number of looks.

The maximum likelihood estimators based on the sample $Z_1,\dots,Z_n$ of random variables are the sample mean $\widehat{\lambda}=n^{-1}\sum_{i=1}^n Z_i$ and the solution of the non-linear equation $\ln\widehat{L}-\psi^0(\widehat{L})-\ln n^{-1}\sum_{i=1}^n Z_i+n^{-1}\sum_{i=1}^n \ln Z_i=0$, where ψ^0 is the digamma function.

Assuming that the intensity follows a Gamma distribution, a maximum likelihood ratio test can be computed, comparing the likelihood of H_0 to the likelihood of H_1. As defined by [1], considering a serie of only two images, the difference of log-likelihood between H_1 and H_0 is $\Delta H_1=L(2\log 2-2\log(1+R)+\log R)$, where $R=\hat{\lambda}_1/\hat{\lambda}_2$ is the ratio of the mean reflectivities.

The equivalent number of looks L was computed in two ways:

1) $GLRT_a$: by maximum likelihood [11],
2) $GLRT_b$: by the sample coefficient of variation $ENL=(\widehat{\mu}/\widehat{\sigma})^2$ [15].

2) $MIMOSA$ [10]: It detects outliers in a bi-dimensional plot of the arithmetic (AM) and geometric means (GM) compared to the predicted joint distributions for Fisher distributed data (amplitude data was obtained from intensity CSK data). In this approach, both the temporal arithmetic mean $AM=(A_1+A_2)/2$ and the temporal geometric mean $GM=(A_1A_2)^{1/2}$ were calculated, where A_1 and A_2 are amplitude bands at times 1 and 2, respectively. The Fisher distribution functions (for both AM and GM) were fitted using the *fitdist* R package.

3) HD based on stochastic distances [11]: Hypothesis test methods are used to quantifying the contrast between regions. Two samples (sliding windows) at different times can be modeled with the random variables Z_1 and Z_2 with densities $f_{Z_1}(z,\theta_1)$ and $f_{Z_2}(z,\theta_2)$ respectively, and parameters $\theta_1=(L_1,\lambda_1)$ and $\theta_2=(L_2,\lambda_2)$. It is possible to obtain tests statistics based on stochastic distances for the hypothesis $H_0:\theta_1=\theta_2$ [16]. We used the Hellinger test statistic under the Gamma model, defined in [11] as:

$$S_{\mathrm{H}}=\frac{8mn}{m+n}\left(1-\frac{2^{\frac{\widehat{L}_1+\widehat{L}_2}{2}}(\widehat{\lambda}_1\widehat{\lambda}_2)^{\frac{\widehat{L}_1+\widehat{L}_2}{4}}}{(\widehat{\lambda}_1+\widehat{\lambda}_2)^{\frac{\widehat{L}_1+\widehat{L}_2}{2}}}\right),$$

which is asymptotically distributed as a χ^2_2 random variable.

B. Performance evaluation

Selected regions of change and no-change between images were chosen to serve as reference. The areas were identified using control sites from three Landsat 5 TM images dated at April 24, June 11 and October 17, 2011 (PATH 224, ROW 78) and a Google Earth image of April 7, 2011.

The following changes types were considered: 1) from vegetation to bare soil, 2) from vegetation to urban cover, 3) from bare soil to plowed soil, 4) from vegetation to flooded. Two no-changes types were identified: 1) native vegetation zones, 2) calm water zones. Evaluation was carried out building ROC curves for each methodology.

III. Results

Fig. 2 presents the change maps derived using $GLRT_a$, $MIMOSA$, and HD methodologies; $GLRT_a$ and $GLRT_b$ produced very similar maps, therefore only the former is shown.

Fig. 3 shows the ROC curves for each method: $GLRT_a$ in red, HD in blue, and $MIMOSA$ in black. $GLRT_a$ and

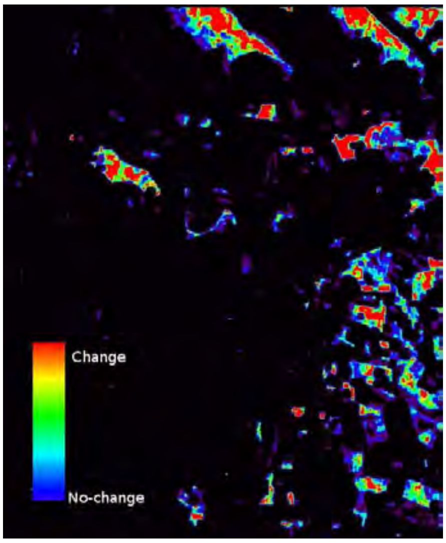

(a) $GLRT_a$

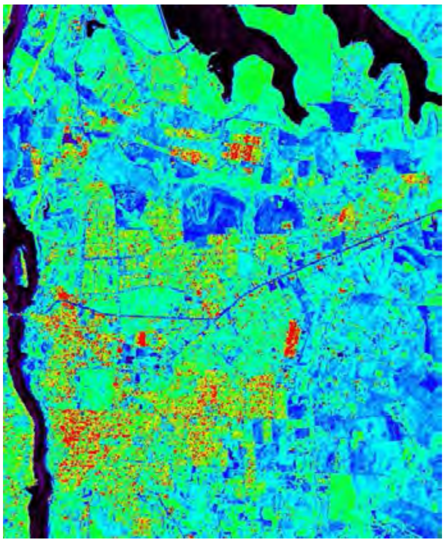

(b) $MIMOSA$

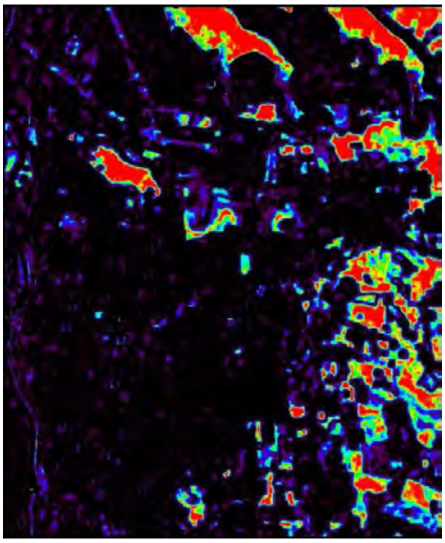

(c) HD

Fig. 2. Change maps. Range values are different but the color scale, shown in (a), is the same.

$GLRT_b$ produced very similar curves, therefore only the former is shown. Both, the corresponding areas under the ROC curves (AUC) and the optimized thresholds are tabulated in Table I. Youden's J statistic [17] was employed in order to find the optimal cut-off: the threshold that maximizes the distance to the identity (diagonal) line. The optimality criterion is, thus, $\max\{\text{sensitivity} + \text{specificity}\}$.

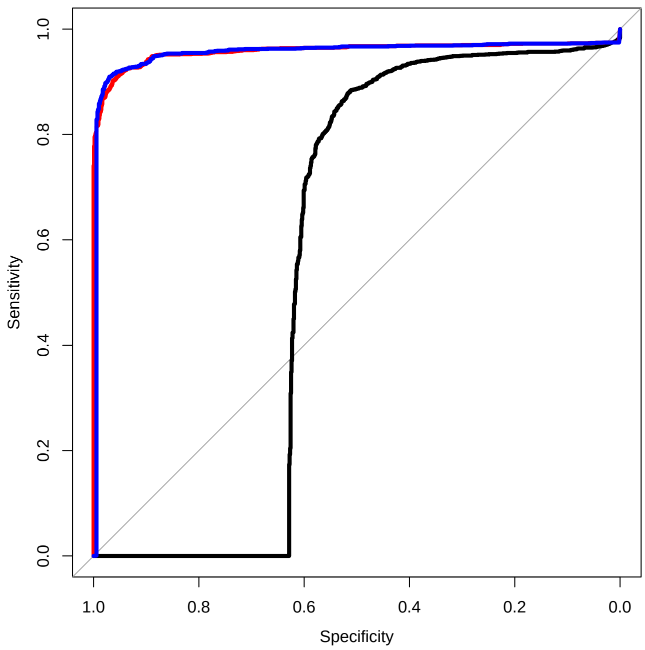

Fig. 3. ROC curves for each methodology. Red curve corresponds to $GLRT_a$ method, black curve to $MIMOSA$, while blue curve to HD method

In order to explain the deficient results obtained with $MIMOSA$, we identified the control regions of change and no-change in the GM–AM scatter plots of the temporal

TABLE I

AREAS UNDER THE ROC CURVES (AUC) AND THE OPTIMIZED THRESHOLDS FOR EACH ASSESSED METHODOLOGY.

Methodology	AUC	Threshold selected
$GLRT_a$	0.959	-1.764
$GLRT_b$	0.954	-1.678
$MIMOSA$	0.569	0.538
HD	0.955	65.908

images. Fig. 4 shows the values of those ground truth pixels that did not change in blue, those ground truth pixels that changed appear in red.

Pixels that did not changed, for example calm water pixels marked as blue, are close to the straight line of slope 1, while the areas that changed have values not very far from this diagonal. In the work by Quin et al. [10], departures from the joint $\mathcal{G}^0$ distribution (which they call "Fisher" [16]), are associated to change but, in our data, such departures were not observed.

IV. Conclusions

Methods based on the Generalized Likelihood Ratio Test and stochastic distances presented similar very good performance. They both are based on the assumption that intensity SAR data can be fitted by Gamma distribution models. The results highlight the use of these methodologies for change detection in CSK data. However, it was observed in the **change maps** obtained with both procedures that homogeneous zones (like calm water bodies) present more sensitivity to small changes. It is possibly due to the better fitting of Gamma model in those areas. Areas with different texture levels will be analyzed using specific and suitable approaches and distributions.

$MIMOSA$ assumes an underlying $\mathcal{G}^0$ distribution for amplitude data, and identifies changes in those observations

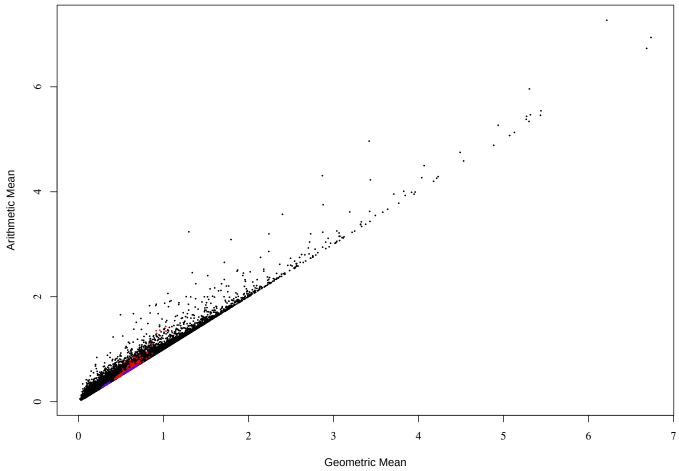

Fig. 4. Change and no-change training pixels in GM–AM scatter plots.

which depart from the diagonal of the GM–AM scatter plot [10]. Pixels aggregated in a given image parcel that shows a certain level of change are not beyond the joint pdf (as demonstrated by their location in the GM–AM scatter plot) as suggested by [10]. In this way, $MIMOSA$ calculation fails at detecting those changes. It seems that this method would be only suitable to detect pixels whose change in amplitude is noticeable, like change from/to urban pixels.

A relevant point to be considered in further works is the way to select optimal window sizes to detect changes. As in any statistically-based image processing procedure, large windows are desired to obtain accurate estimates, but small windows are required in order to grant observations without contamination. Moreover, a future issue is to improve threshold determination on **change maps**. It would be also interesting to assess the relationship between the optimized thresholds here obtained and the different change types defined.

References

[1] M. M. Horta, N. D. A. Mascarenhas, H. Sportouche, N. Seichepine, F. Tupin, and J. M. Nicolas, "Change detection in multitemporal HR SAR images: a hypothesis test-based approach.," in *Geoscience and Remote Sensing Symposium (IGARSS), 2012 IEEE International*, 2012.

[2] Y. Bazi, L. Bruzzone, and F. Melgani, "An unsupervised approach based on the generalized Gaussian model to automatic change detection in multitemporal SAR images," *IEEE Transactions on Geoscience and Remote Sensing*, vol. 43, pp. 874–887, 2005.

[3] F. Bovolo, C. Marin, and L. Bruzzone, "A novel hierarchical approach to change detection with very high resolution SAR images for surveillance applications," in *Geoscience and Remote Sensing Symposium (IGARSS), 2012 IEEE International*, 2012, pp. 1992–1995.

[4] J. Inglada and G. Mercier, "A new statistical similarity measure for change detection in multitemporal SAR images and its extension to multiscale change analysis," *IEEE Transactions on Geoscience and Remote Sensing*, vol. 45, no. 5, pp. 1432–1445, 2007.

[5] F. Bujor, E. Trouve, L. Valet, J-M Nicolas, and J.-P. Rudant, "Applications of log-cumulants to the detection of spatiotemporal discontinuities in multitemporal SAR images," *IEEE Transactions on Geoscience and Remote Sensing*, vol. 42, no. 10, pp. 2073–2084, 2004.

[6] F.T. Ulaby, F. Kouyate, B. Brisco, and T.H.L. Williams, "Textural information in SAR images," *IEEE Transactions on Geoscience and Remote Sensing*, vol. GE–4, no. 2, pp. 235–245, Mar 1986.

[7] P. Lombardo and C. J. Olivier, "Maximum likelihood approach to the detection of changes between multitemporal SAR images," *IEE Proceedings in Radar, Sonar and Navigation*, vol. 148, no. 4, pp. 200–210, 2001.

[8] L. Alparone, B. Aiazzi, S. Baronti, A. Garzelli, and F. Nencini, "Robust change analysis of SAR data through information-theoretic multitemporal features," *IEEE International Geoscience and Remote Sensing Symposium (IGARSS)*, pp. 3883–3886, 2007.

[9] B. Aiazzi, L. Alparone, S. Baronti, A. Garzelli, and C. Zoppetti, "A robust change detection feature for Cosmo-Skymed detected SAR images," in *6th International Workshop on the Analysis of Multi-temporal Remote Sensing Images (Multi-Temp)*, 2011, pp. 125–128.

[10] G. Quin, B. Pinel-Puyssegur, and J.-M. Nicolas, "Comparison of harmonic, geometric and arithmetic means for change detection in SAR time series," in *9th European Conference on Synthetic Aperture Radar (EUSAR)*, 2012, pp. 255–258.

[11] S. Lanfri, G. Palacio, M. Lanfri, M. Scavuzzo, and A. C. Frery, "Information content in COSMO-SkyMed data," in *IEEE International Geoscience and Remote Sensing Symposium (IGARSS)*, 2013.

[12] R Core Team, *R: A Language and Environment for Statistical Computing*, R Foundation for Statistical Computing, Vienna, Austria, 2013, ISBN 3-900051-07-0.

[13] G. Gao, "Statistical Modeling of SAR images: A Survey," *Sensors*, vol. 10, pp. 775–795, 2010.

[14] L. Torres, T. Cavalcante, and A. C. Frery, "Speckle reduction using stochastic distances," in *CIARP 2012 – Progress in Pattern Recognition, Image Analysis, Computer Vision, and Applications*, L. Alvarez, M. Mejail, L. Gomez, and J. Jacobo, Eds. 2012, vol. 7441 of *Lecture Notes in Computer Science*, pp. 632–639, Springer Berlin / Heidelberg.

[15] A. Shamsoddini and C. J. Trinder, "Edge-detection-based filter for SAR speckle noise reduction," *International Journal of Remote Sensing*, vol. 33, pp. 2296–2320, 2011.

[16] A. D. C. Nascimento, R. J. Cintra, and A. C. Frery, "Hypothesis testing in speckled data with stochastic distances," *IEEE Transactions on Geoscience and Remote Sensing*, vol. 48, no. 1, pp. 373–385, 2010.

[17] W. J. Youden, "Index for rating diagnostic tests," *Cancer*, vol. 3, pp. 32–35, 1950.